Cycloaddition of CO₂ to Epichlorohydrin over Pyridine, Vinylpyridine, and Poly(vinylpyridine): The Influence of Steric Crowding on the Reaction Mechanism

Renxi Jin, 1† Hui Xu, 2† Justin Easa, 1 Alejandro Chapero-Planell, 1 Casey P. O'Brien 1*

¹Department of Chemical and Biomolecular Engineering, University of Notre Dame, Notre Dame, IN, 46556, USA

²Department of Chemistry and Biochemistry, University of Notre Dame, Notre Dame, IN, 46556, USA

†Equal contribution

*Corresponding author. E-mail address: cobrie23@nd.edu

Abstract

The cycloaddition of CO₂ with epoxides is a 100% atom economical reaction that utilizes CO₂ and produces valuable cyclic carbonate products. Organic bases are attractive catalysts for this reaction because of their green characteristics, such as low cost and low toxicity. However, further catalyst development is required to achieve acceptable yields at mild temperatures and pressures. This work aims to establish catalyst structure-performance relationships to accelerate the rational design of high performance organic base catalysts for the cycloaddition reaction. Towards this end, we investigate the influence of steric crowding at the ring nitrogen atom of a series of pyridine-based catalysts on the reaction mechanism and catalyst performance using batch reactor measurements at mild temperature (57 °C) and atmospheric pressure under solvent-less conditions combined with *in-situ* infrared spectroscopic characterization of the catalysts. We show that steric crowding at the ring nitrogen atom has a significant influence on the reaction mechanism and catalyst performance. Catalysts with unhindered access to the ring nitrogen atom, such as pyridine, 4-vinylpyridine, 3-vinylpyridine, and poly(4-vinylpyridine), are completely transformed during the cycloaddition

reaction by quaternization from the epoxide reactant, producing zwitterionic pyridinium-epoxide adducts and ammonium salts that precipitate out of solution. Catalysts with hindered access to the ring nitrogen atom, such as 2-vinylpyridine and poly(2-vinylpyridine), resist quaternization from the epoxide reactant due to the high degree of steric hindrance at the ring nitrogen atom. The poly(2-vinylpyridine) catalyst in particular displayed high stability, high product selectivity, and high activity for cyclic carbonate synthesis. These molecular-level insights have significant implications for the rational design of active, stable, and metal-free catalysts for cyclic carbonate synthesis by tuning the steric crowding at the active site.

1. Introduction

Synthesis of cyclic carbonates from the cycloaddition of CO₂ with epoxides is an attractive green reaction that is 100% atom economical and it utilizes CO₂. 1-2 Cyclic carbonates are also industrially valuable chemicals used as polar aprotic solvents, 3-5 as electrolytes for lithium batteries, ⁶ and as chemical intermediates for synthesis of fine chemicals ⁷⁻⁹ and polymers. ¹⁰⁻¹³ The cycloaddition reaction is thermodynamically favorable at mild temperatures and pressures, ¹⁴ but a suitable catalyst is required to reduce the activation barrier. 14-15 Many different types of homogeneous and heterogeneous catalysts have been used to carry out the cycloaddition reaction, including metal oxides, 16-17 ammonium salts, 15, 18-19 ionic liquids, 15, 20-24 transition metal complexes, 25-27 functional polymers, 17, 28-32 amines or organic bases, 1, 33-39 and metal-organic frameworks. 17, 40-41 From a green chemistry perspective, current focus is on the development of metal-free and halogen-free catalysts that can catalyze the reaction at mild temperatures and pressures without co-catalysts or solvents.^{2,14} Organic N-nucleophilic base catalysts are promising metal- and halogen-free catalysts for the cycloaddition reaction because of their nucleophilic and basic nitrogen atoms that can activate CO₂ and facilitate epoxide ring opening, and because of their highly tunable catalytic properties.^{2, 34, 42} However, there is still a need to develop organic Nnucleophilic base catalysts with high activity for cyclic carbonate synthesis at mild temperatures and pressures without metals and halogens.²

In order to rationally design high performance organic N-nucleophilic base catalysts, it is critical to identify and understand the structural features that determine its catalytic performance, including catalyst stability. N-nucleophilicity is generally considered an important structural parameter that determines the performance of organic base catalysts.^{2, 15, 34, 43} Natongchai et al.³⁴ systematically investigated the effect of N-nucleophilicity within a series of 4-aminopyridine

catalysts (e.g., pyridine, 4-dimethylaminopyridine (DMAP), 9-azajulolidine, Triazabicyclodecene (TBD)) on their activity for CO₂ cycloaddition. These compounds were selected for their study because they have comparable structures, with pyridinic nitrogen atoms, and their nucleophilicity can be strongly tuned and enhanced by amino substitution at the 4- position of the pyridine moiety. They showed that the catalytic performance of certain 4-aminopyridines surpassed that of traditional N-nucleophiles such as DMAP and TBD. They further showed that the catalytic performance of 4-aminopyridines can be predicted by calculating the carbon basicities of the catalysts towards the epoxide substrate.

There are at least four factors that contribute to the nucleophilicity of organic N-nucleophilic base catalysts: charge, electronegativity, solvent, and steric hindrance. In this work, we systematically investigate the influence of steric hindrance on the mechanism of cyclic carbonate synthesis over a series of pyridine-based catalysts (see **Figure 1**): pyridine, 2-vinylpyridine (2VP), 3-vinylpyridine (3VP), 4-vinylpyridine (4VP), poly(2-vinylpyridine) (P2VP), and poly(4-vinylpyridine) (P4VP). This series of catalysts is selected for this study because their pyridinic nitrogen active sites are similar, but the degree of steric hindrance at the N-nucleophile site varies significantly. The N-nucleophile sites of 2VP and P2VP are much more sterically crowded than that of pyridine, 4VP, 3VP, and P4VP, because of their close proximity to the vinyl group (4VP and 3VP) and the polymer backbone (P4VP).

(a) Pyridine (b) 4VP (c) P4VP (d) 3VP (e) 2VP (f) P2VP

Figure 1. Chemical structures of (a) pyridine, (b) 4VP, (c) P4VP, (d) 3VP, (e) 2VP, and (f) P2VP, in order of increasing steric hindrance at the nucleophilic nitrogen active site.

This work demonstrates that steric crowding at the N-nucleophile site of pyridine-based catalysts does indeed have a significant impact on the reaction mechanism and catalyst performance. More specifically, we demonstrate that the unhindered N-nucleophile sites of pyridine, 4VP, 3VP, and P4VP catalysts are completely quaternized by the epoxide reactant, forming a solid that precipitates out of the reaction solution. The sterically hindered N-nucleophile sites of 2VP and P2VP, on the other hand, resist quaternization by the epoxide due to the high degree of steric hindrance at the nitrogen active site. The solid precipitates formed in the pyridine, 4VP, 3VP, and P4VP reaction solutions all have similar structures and are catalytically active for the cycloaddition reaction. However, the mechanism of cyclic carbonate synthesis over the quaternized variants of pyridine, 4VP, 3VP, and P4VP are different than that of 2VP and P2VP.

2. Experimental

Chemicals. 2-Vinylpyridine (≥97.0% stabilized, VWR) and 4-Vinylpyridine (95% stabilized, Sigma-Aldrich) were purified by distillation before use. Other chemicals used in this work were utilized without further purification: 3-vinylpyridine (>96.0% purity, TCI), pyridine (GR ACS, Sigma-Aldrich), poly(2-vinylpyridine) of 95-100% purity and ~40,000 MW (Polysciences Inc.), poly(4-vinylpyridine) (purity not specified) of ~60,000 MW (Sigma-Aldrich),

epichlorohydrin of ≥99% purity (Sigma-Aldrich), 1,3,5-trimethoxybenzene of ≥99% purity (Sigma-Aldrich), chloroform-d of ≥99.8% purity (Isotopic, BeanTown chemical) contains 1% tetramethylsilane (TMS).

Procedure for Cyclic Carbonate Synthesis in a Batch Reactor. The cycloaddition reaction of CO₂ into epoxide was evaluated in a 25 mL Schlenk tube. 5 ml of epichlorohydrin (ECH) and 100 mg of polymer were mixed with magnetic stirring bar. 0.1 g of 1,3,5-trimethoxybenzene was then added in the mixture as an internal standard. The flask was purged with CO₂ three times and connected with a CO₂ gas bag. The flask was then heated to 57 °C with a thermostatic oil bath. After 24 hours, the flask was removed from the oil bath and quickly cooled down to room temperature, the liquid-phase products were collected after filtering out the precipitate (for P4VP, 4VP, 3VP, 2VP, and pyridine). The epoxide and carbonate concentrations were determined by analyzing the liquid-phase products with ¹H-NMR (Bruker AVANCE III HD 400 Nanobay spectrometer) using chloroform-d as a solvent at room temperature. All reactions were repeated four times and all reaction metrics (mass of precipitate, conversion, selectivity, carbonate production rate) are reported as averages and standard deviations of the results from the four different runs.

A significant amount of swelling of the rubber sleeve stopper used to seal the reactor was observed over the course of the cycloaddition reaction. The swelling is most likely due to the absorption of volatile epichlorohydrin into the rubber. We used a 25 mL Schlenk tube with a small area of exposed rubber to minimize this swelling effect (see Figure S1). To account for this loss of reactant into the rubber stopper, the mass of the rubber stopper was weighed before and after the reaction. The mass gain of the rubber stopper was roughly the same for all different catalysts

(see Figure S2), and was approximately 4 ± 2 mg. This reactant loss into the rubber stopper was accounted for in our calculation of conversion and selectivity.

The epichlorohydrin conversion was calculated according to the following equation:

$$Conversion = \frac{[Epi.\ at\ t=0\ h] - [Epi.\ evap.\,] - [Epi.\ at\ t=24\ h]}{[Epi.\ at\ t=0\ h] - [Epi.\ evap.\,]} \times 100\%$$

where $[Epi.\ at\ t=0\ h]$ and $[Epi.\ at\ t=24\ h]$ represent the moles of epichlorohydrin at t=0 h and 24 h of reaction, respectively, and $[Epi.\ evap.]$ represent moles of epichlorohydrin evaporated and absorbed by the rubber stopper. The amount of epichlorohydrin evaporated into the rubber stopper was estimated by measuring the mass change of the rubber stopper over the course of the reaction. The moles of the chloroprene carbonate product and the epichlorohydrin reactant at t=0 h and at t=24 h were determined from the 1 H-NMR spectra. The selectivity towards the chloroprene carbonate product was calculated according to the following equation:

$$Selectivity = \frac{[Carbonate]}{[Epi. at t = 0 h] - [Epi. evap.] - [Epi. at t = 24 h]} \times 100\%$$

where [Carbonate] represents the moles of chloroprene carbonate produced after 24 h of reaction, and all of the other variables are defined above. Note that this is a different method for calculating selectivity than is typically reported in the literature. In the literature, selectivity is typically calculated relative to the different liquid-phase products (e.g., 1,2-diols³⁴) that are detected by NMR. In this work, we did not observe any products other than chloroprene carbonate in the liquid phase, so based on the common method for determining selectivity in the literature, the selectivity of all catalysts reported in this work was >99%. Our calculation of selectivity is relative to the change in the number of moles of the epichlorohydrin reactant (i.e. the denominator in the

'Selectivity' equation), and our reported selectivities are lower than is typically reported in the literature.

Infrared Spectroscopy. Attenuated Total Reflection Infrared (ATR-IR) analysis was used to characterize the molecular structure of solid precipitates formed during the cycloaddition reaction. ATR-IR measurements were performed on a Jasco FT-IR-6300 spectrometer in attenuated total reflection mode with a spectral resolution of 4 cm⁻¹ and 64 scans-per-spectrum.

In-situ PM-IRAS. In-situ PM-IRAS measurements were performed using an experimental apparatus has been described in detail in a previous publication.⁴⁵ Briefly, the experimental apparatus consists of a Bruker Vertex 70 FTIR spectrometer with a Bruker PMA50XL external accessory and a liquid nitrogen cooled MCT detector. A Harrick RefractorReactorTM grazing angle accessory was positioned in the sample compartment of the PMA50XL external accessory. P4VP and P2VP thin films were prepared for in-situ PM-IRAS characterization by knife casting (Gardner Digital Microm II Film Applicator; blade height was set to 10 micrometers) from approximately 20 wt% solutions onto 1"x 1" gold coated microscope slides and drying under the lab atmosphere. The coated slides were installed in the Harrick RefractorReactorTM. Following installation, the reactor was purged with Ar (Airgas, 99.999%), and a baseline spectrum was collected. After background spectrum collection, an epichlorohydrin/CO₂/N₂ gas mixture was introduced to the reactor by bubbling a 20% CO₂ (Airgas, 99.995 %) in balance N₂ gas mixture through liquid epichlorohydrin at ~20°C. Aalborg mass flow controllers regulated the flow rates of the CO₂ and N₂ feed gases to give a total CO₂+N₂ flow rate of 100 mL/min. We estimate that the partial pressure of epichlorohydrin in the resulting gas mixture was ~1.6 kPa with ~20 kPa CO₂ and ~80 kPa N₂. PM-IRAS measurements were performed continuously during exposure of P4VP or P2VP to the epichlorohydrin/CO₂/N₂ gas mixture with a spectral resolution of 4 cm⁻¹, 2 min-per-scan,

and the photoelastic modulator setting of 1300 cm⁻¹. Heating cartridges positioned below the sample stage of the RefractorReactorTM were used to heat the sample to the desired temperature (57 °C), which was measured using a type K thermocouple fixed to the sample surface using the reactor's sample holders.

3. Results and Discussion

3.1. Chloroprene Carbonate Synthesis over P4VP, P2VP, 4VP, 3VP, 2VP, and Pyridine

The cycloaddition of CO₂ with epichlorohydrin over P4VP, P2VP, 4VP, 3VP, 2VP, and pyridine was evaluated in a batch reactor at 57 °C under atmospheric pressure of CO₂ for 24 hours. Approximately 100 mg of each catalyst was initially dissolved in the epichlorohydrin solution without solvent to form a transparent solution. After 24 h of reaction, a large amount of bulky dark green solid precipitate was observed in the P4VP, 4VP, 3VP, and pyridine reaction solutions. No precipitate formed in the P2VP batch reactor after 24 h of reaction, and only a small amount of precipitate was observed in the 2VP reaction solution, although both the P2VP and 2VP solutions did change to a light orange color. Figure S3 in the Supporting information shows photographs of the P4VP, P2VP, 4VP, 2VP, 3VP, and pyridine reaction solutions before and after reaction.

The solid precipitate formed in the P4VP, 4VP, 3VP, 2VP and pyridine reaction solutions was separated from the liquid by centrifugation, and the solid was washed with acetone three times to remove residual chloroprene carbonate product. After drying in a vacuum oven overnight, the mass of the solid precipitate was measured. **Figure 2(a)** shows the mass of precipitate formed in the P4VP, P2VP, 4VP, 3VP, 2VP, and pyridine reaction solutions and **Table 1** summarizes the results. The 4VP reaction solution formed the largest amount of precipitate, and the amount of precipitate formed decreased in the following order: $4\text{VP} (0.32 \pm 0.03 \text{ g}) > \text{P4VP} (0.22 \pm 0.09 \text{ g}) > \text{P4VP} (0.21 \pm 0.09 \text{ g}) > \text{P4VP} (0.11 \pm 0.01 \text{ g}) > \text{P4VP} (0.11 \pm$

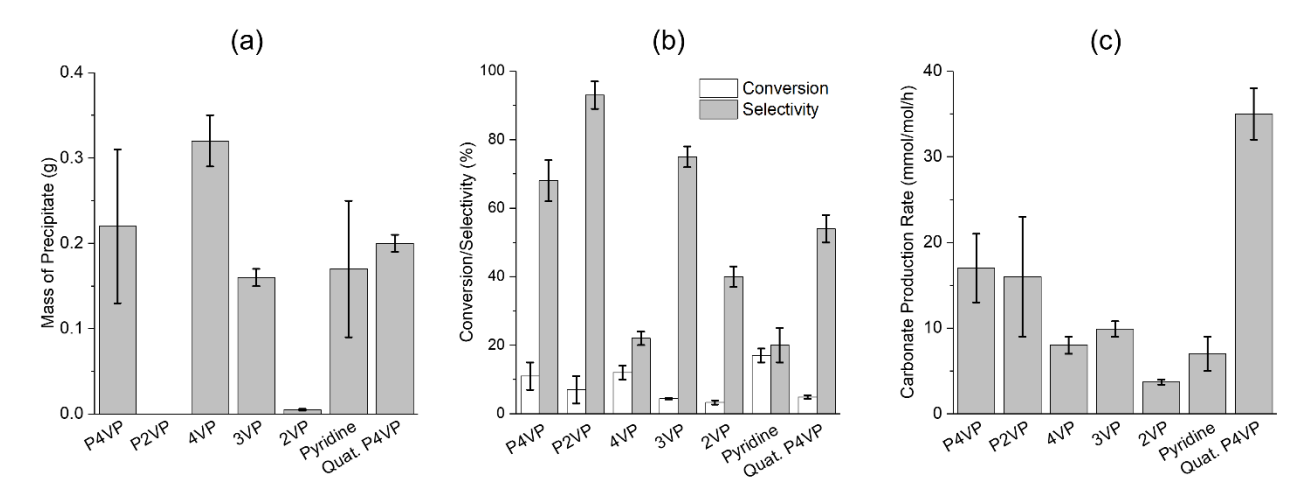


Figure 2. (a) Mass of solid precipitate formed, (b) epichlorohydrin conversion and chloroprene carbonate product selectivity, and (c) chloroprene carbonate production rate during the cycloaddition of CO₂ with epichlorohydrin over 100 mg of P4VP, P2VP, 4VP, 3VP, 2VP, pyridine, and P4VP quaternized with epichlorohydrin (without CO₂) at 57 °C with 1 atm CO₂ for 24 h.

Table 1. Epichlorohydrin conversion (%), chloroprene carbonate selectivity (%), precipitate mass (g), and chloroprene carbonate production rate (mmol of product per mol of N active site per hour) of P4VP, P2VP, 4VP, 3VP, 2VP, pyridine, and P4VP quaternized with epichlorohydrin (without CO₂) after 24 hours of the CO₂ cycloaddition with epichlorohydrin reaction at 57 °C and 1 atm CO₂. The values listed are averages and standard deviations of four different reactions repeated under identical conditions.

Catalyst	Conversion (%)	Selectivity (%)	Precipitate Mass (g)	Carbonate Production Rate (mmol/mol/h)
P4VP	11 ± 4	68 ± 6	0.22 ± 0.09	17 ± 4
P2VP	7 ± 4	93 ± 4	_	16 ± 7
4VP	12 ± 2	22 ± 2	0.32 ± 0.03	8 ± 1
3VP	4.4 ± 0.2	75 ± 3	0.16 ± 0.01	9.9 ± 0.9
2VP	3.3 ± 0.6	40 ± 3	0.005 ± 0.001	3.7 ± 0.3
Pyridine	17 ± 2	20 ± 5	0.17 ± 0.08	7 ± 2
Quat. P4VP	4.9 ± 0.5	54 ± 4	0.20 ± 0.01	35 ± 3

The liquid-phase reaction solutions, excluding insoluble solid precipitates, were analyzed by proton nuclear magnetic resonance (¹H-NMR) spectroscopy to determine the reactant conversion, product selectivity, and chloroprene carbonate production rate. The ¹H-NMR spectra before and after reaction are shown in Figures S4 through S9. Interestingly, the ¹H-NMR spectra

of the P4VP, 4VP, 3VP, and pyridine reaction solutions after 24 h of reaction did not show any peaks associated with the P4VP, 4VP, 3VP, or pyridine catalysts, respectively. Not coincidentally, these P4VP, 4VP, 3VP, and pyridine reaction solutions also formed large amounts of solid precipitate (see Figure 2(a) and Table 1). In contrast, the ¹H-NMR spectra of the P2VP and 2VP reaction solutions collected after 24 h of reaction showed clear peaks associated with the P2VP and 2VP catalysts. There was little to no solid precipitate observed in these P2VP and 2VP reactions solutions. Thus, there appears to be a correlation between catalyst stability and solid precipitate formation. The P2VP and 2VP catalysts were stable and remained in the liquid phase during the entire course of the reaction with little or no precipitate formation. The P4VP, 4VP, 3VP, and pyridine catalysts, on the other hand, were unstable and large amounts of solid precipitate were observed. This observation suggests that the P4VP, 4VP, 3VP, and pyridine catalysts are transformed into the solid precipitate during the course of the reaction, and the P2VP and 2VP catalysts are much more resistant to this transformation.

The epichlorohydrin conversion (**Figure 2(b)**) decreases in the following order: pyridine $(17\pm2\%)>4$ VP $(12\pm2\%)>$ P4VP $(11\pm4\%)>$ P2VP $(7\pm4\%)>3$ VP $(4.4\pm0.2\%)>$ 2VP $(3.3\pm0.6\%)$. The epichlorohydrin conversion is generally higher for the catalysts that formed a large amount of solid precipitate (pyridine, P4VP, 4VP) than the catalysts that formed little or no solid precipitate (P2VP, 2VP). This may indicate that a significant amount of the epichlorohydrin reactant is incorporated into the solid precipitate and thus the catalysts that formed large amounts of solid precipitate also displayed higher epichlorohydrin conversions than catalysts that formed little or no precipitates. The high conversion of pyridine relative to the P4VP and 4VP catalysts is at least partially the result of the higher number of N active sites in the pyridine reaction solution. A constant catalyst mass (100 mg) was used for all catalysts used, and pyridine has a lower

molecular weight (79 g/mol) than the other catalysts, which all had a molecular weight of 105 g/mol, and hence \sim 25% more N active sites per unit mass of pyridine.

The chloroprene carbonate product selectivity, plotted in **Figure 2(b)**, was highest over the P2VP catalyst and decreases in the order P2VP ($93 \pm 4\%$) > 3VP ($75 \pm 3\%$) \approx P4VP ($68 \pm 6\%$) > 2VP ($40 \pm 3\%$) > 4VP ($22 \pm 2\%$) \approx Pyridine ($20 \pm 5\%$). The P2VP catalyst exhibited the highest chloroprene carbonate selectivity because no solid precipitate was formed and no other products were detected by 1 H-NMR spectroscopy. It is unclear why the 2VP catalyst displayed a low product selectivity ($40 \pm 3\%$); no other products were detected in the 2VP reaction solution by 1 H-NMR spectroscopy except for chloroprene carbonate, and only a very small amount of the solid precipitate was formed. It is possible that a significant amount of the chloroprene carbonate product is incorporated into the small amount of solid precipitate formed in the 2VP reaction solution, which would not be detectable by 1 H-NMR spectroscopy and would thus decrease the calculated selectivity. It is also possible that some other product was formed in the 2VP solution that was not soluble in the CDCl₃ solvent used for 1 H-NMR analysis, and thus the low selectivity of 2VP could be due to the formation of some insoluble product.

Figure 2(c) shows the chloroprene carbonate production rate over the different catalysts, which was normalized by the number of N active sites in the catalyst and is given in units of mmol of chloroprene carbonate product per mol of N active sites per hour (mmol/mol/h). The chloroprene carbonate production rate over the polymeric catalysts P4VP ($17 \pm 4 \text{ mmol/mol/h}$) and P2VP ($16 \pm 7 \text{ mmol/mol/h}$) are essentially the same, within experimental error, and are both significantly greater than that of 4VP ($8 \pm 1 \text{ mmol/mol/h}$), 2VP ($3.7 \pm 0.3 \text{ mmol/mol/h}$), 3VP ($9.9 \pm 0.9 \text{ mmol/mol/h}$), and pyridine ($7 \pm 2 \text{ mmol/mol/h}$). This trend in production appears to correlate with the nucleophilicity, or basicity (pK_a), of the catalyst as one might expect for the cycloaddition

reaction.³⁴ pK_a is often used as a metric to quantify basicity or nucleophilicity; the larger the pK_a is, the more basic it is and stronger bases are usually stronger nucleophiles. Values for pK_a of P4VP, P2VP, and 3VP are sparse in the literature and inconsistent, but reliable pKa values for pyridine (pK_a = 5.22), 4VP (pK_a = 5.5), and 2VP (pK_a = 4.98) have been reported in the literature.⁴⁶ The order of increasing production rate (2VP < pyridine < 4VP) follows the order of increasing basicity/nucleophilicity (2VP < pyridine < 4VP).

Tantavichet et al.⁴⁷ reported a pK_a of 4.5 for P2VP and Chanda et al.⁴⁸ reported a pK_a of 5.8 for P4VP. While this trend is consistent with the trend in the pK_a's of 2VP (4.98) and 4VP (5.5), it is inconsistent with spectroscopic and theoretical calculations by Matsuo et al.⁴⁹ of P4VP and P2VP that show P2VP has a higher ability for electron donation and thus a higher pK_a value for P2VP would be expected. As an approximation, the methyl groups of 2-methylpyridine and 4-methylpyridine can be considered as analogous to the polymer backbones of P2VP and P4VP. The pK_a values of 2-methylpyridine (5.96)⁴⁶ and 4-methylpyridine (5.98)⁴⁶ are approximately the same and higher than 2VP, 4VP, and pyridine. These values are more in line with expectations that the polymer chain is an electron-donating group that should increase the pK_a value relative to pyridine.

The high pK_a of P2VP, P4VP, and 3VP could explain the high chloroprene carbonate production rate of these catalysts relative to the other catalysts with lower pK_a values and lower carbonate production rates. If we assume these values for the pK_a of P2VP (5.96) and P4VP (5.98), and if we assume that the pK_a of 3VP is similar to that of 3-methylpyridine (5.63⁵⁰), then there does appear to be a strong correlation between pK_a and chloroprene carbonate production rate (see Figure S11) for this set of pyridine, vinylpyridine, and poly-vinylpyridine catalysts.

3.2. Characterization of the Solid Precipitate

In the previous section, we demonstrated that P4VP, 4VP, 3VP, and pyridine catalysts are completely transformed into a solid precipitate during the cycloaddition reaction, whereas the P2VP and 2VP catalysts are much more resistant to precipitate formation. This transformation of the catalyst into solid precipitates has important consequences for the activity and selectivity of the catalyst, and thus it is important to understand this process. In this section, we analyze the composition of the solid precipitate formed in the P4VP, 4VP, 3VP, 2VP and pyridine reaction solutions to shed more light on the catalyst performances.

To determine the molecular structure of the solid precipitate formed in the P4VP, 4VP, 3VP, 2VP, and pyridine reaction solutions, the solid precipitates were dried and analyzed by ATR-IR spectroscopy. Figure 3 shows the ATR-IR spectrum of (a) pristing P4VP and (b) the solid precipitate formed in the P4VP reaction solution. The ATR-IR spectrum of pristine P4VP shows characteristic bands of the pyridine ring at 1597, 1556, 1494, 1454, and 1415 cm⁻¹. ⁵¹⁻⁵² The ATR-IR spectrum of the crude solid precipitate does not show any of these characteristic pyridine bands; instead, there are three intense absorption bands at 1790, 1165, and 1067 cm⁻¹ and several weaker bands in the 1630-1260 cm⁻¹ range. Most of these bands can be assigned to the chloroprene carbonate product. To verify this assignment, we collected the ATR-IR spectrum of lab-made pure chloroprene carbonate product (see Section S5 for details), shown in Figure 3(c)), for comparison to that of the solid precipitate formed in the P4VP reaction solution. At first glance, the ATR-IR spectrum of the purified chloroprene carbonate product appears nearly identical to that of the solid precipitate. However, chloroprene carbonate is soluble in epichlorohydrin, and therefore the solid precipitate is not pure chloroprene carbonate, but likely some compound that contains chloroprene carbonate.

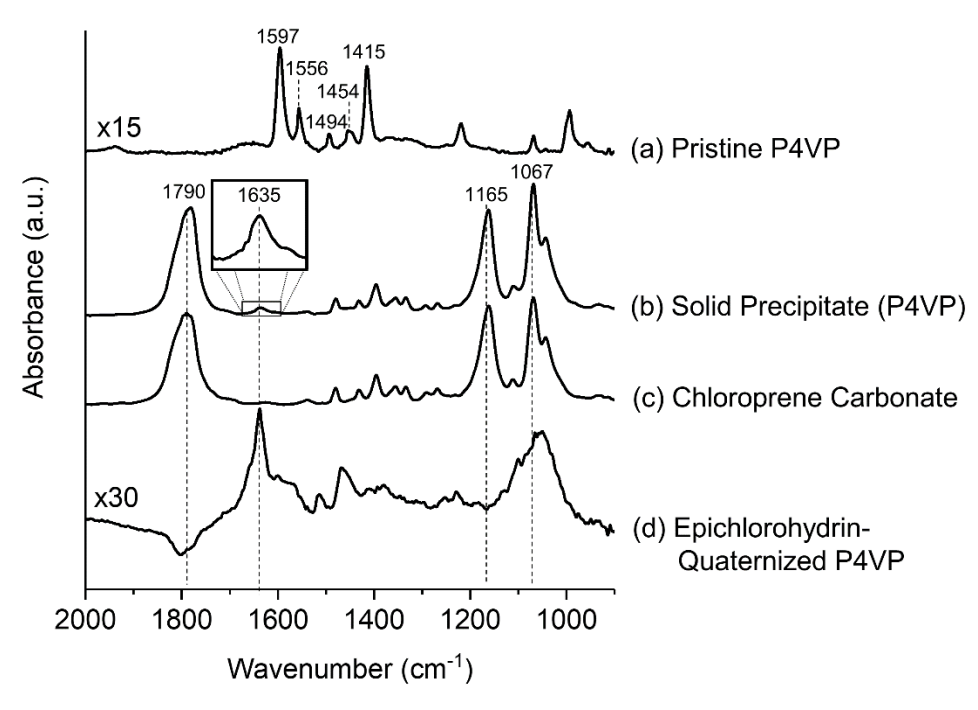


Figure 3. ATR-IR spectra of (a) pristine P4VP, (b) the solid precipitate collected from the post-reaction P4VP solution, (c) the pure chloroprene carbonate product, and (d) P4VP quaternized by epichlorohydrin at 57 °C without CO₂.

In addition to the characteristic bands associated with the chloroprene carbonate product, the ATR-IR spectrum of the solid precipitate (**Figure 3(b)**) displays a weak absorption band centered at ~1635 cm⁻¹ (see inset) that is not present in the ATR-IR spectrum of the purified chloroprene carbonate. This band at ~1635 cm⁻¹ is most likely associated with a ring-stretching vibration of a pyridinium ion resulting from quaternization of P4VP with epichlorohydrin. ^{51, 53-55} To verify this assignment, we quaternized P4VP using epichlorohydrin *without* CO₂ at 57 °C, which produced a solid green precipitate very similar in appearance to the solid precipitate formed during the cycloaddition reaction over P4VP. **Figure 3(d)** shows the ATR-IR spectrum of the epichlorohydrin-quaternized P4VP, which shows an absorption band centered at ~1635 cm⁻¹. This supports our assignment of the band at 1635 cm⁻¹ to epichlorohydrin-quaternized P4VP. This band appears very weak in the ATR-IR spectrum of the solid precipitate because the absorption bands associated with the chloroprene carbonate product are much stronger than that of the quaternized

P4VP (the absorbance of the quaternized P4VP is multiplied by a factor of 30 in Figure 3 for comparison to the much stronger bands in the solid precipitate and pure chloroprene carbonate).

The solid precipitates formed during the cycloaddition reaction over P4VP, 4VP, 3VP, 2VP, and pyridine were analyzed by ATR-IR spectroscopy after washing with acetone to remove most of the chloroprene carbonate product. **Figure 4** shows the ATR-IR spectra of the washed solid precipitates formed in the P4VP, 4VP, 3VP, 2VP, and pyridine reaction solutions. The ATR-IR spectra of the precipitates formed in the P4VP, 4VP, 3VP, 2VP and pyridine reaction solutions display similar features to each other and to the ATR-IR spectrum of P4VP quaternized by epichlorohydrin without CO₂ (Figure 3(d)). This suggests that the precipitates formed in the different reaction solutions are all most likely quaternary compounds resulting from the quaternization of P4VP, 4VP, 3VP, 2VP, and pyridine by epichlorohydrin.

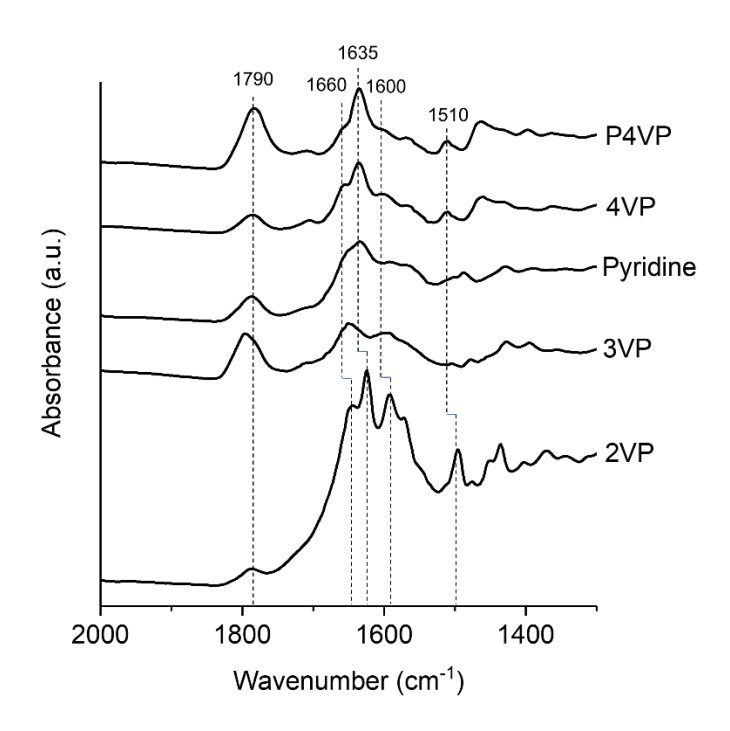


Figure 4. ATR-IR spectra of the solid precipitates formed in the P4VP, 4VP, 2VP, 3VP, and pyridine reaction solutions during the cycloaddition reaction at 57 °C and 1 atm CO₂. The solid precipitates were washed with acetone to remove chloroprene carbonate product, and dried.

All spectra in Figure 4 display a peak at 1790 cm⁻¹, which is associated with residual chloroprene carbonate that was not completely washed away by acetone, and an intense peak at ~1635 cm⁻¹ with a shoulder at ~1660 cm⁻¹ (these peaks are red-shifted by ~10 cm⁻¹ for 2VP). The peak at ~1635 cm⁻¹ and the shoulder at ~1660 cm⁻¹ are both likely associated with pyridinum ring vibrations from epichlorhydrin-quaternized pyridine rings, but with different adducts attached the nitrogen atom of the pyridinium ring. The position of the peak at ~1660 cm⁻¹ is consistent with a zwitterionic pyridinium-epoxide adduct,³⁸⁻³⁹ and the position of the peak at ~1635 cm⁻¹ is consistent with a pyridinium-chlorine quaternary ammonium salt (see **Scheme 1**).³⁸⁻³⁹

Scheme 1. Proposed chemical structures of the solid precipitates formed in the P4VP, 4VP, and pyridine reaction solutions: pyridinium-chlorine quaternary ammonium salt with a characteristic infrared peak at ~ 1635 cm⁻¹, and zwitterionic pyridinium-epoxide adduct with a characteristic infrared peak at ~ 1660 cm⁻¹.

To verify that the peak at ~1635 cm⁻¹ in the ATR-IR spectra of the solid precipitates (Figure 4) is associated with a pyridinium-chlorine quaternary ammonium salt, we quaternized P4VP with HCl (see Section S6 for details). The PM-IRAS spectrum of HCl-quaternized P4VP shows three sharp peaks centered at 1633 cm⁻¹, 1601 cm⁻¹, and 1502 cm⁻¹, which are very similar in position to the bands observed in the ATR-IR spectra of the solid precipitates at ~1635 cm⁻¹, ~1600 cm⁻¹, and

~1510 cm⁻¹ (Figure 4). Thus, the bands at 1635 cm⁻¹, 1601 cm⁻¹, and 1513 cm⁻¹ in the ATR-IR spectra of the solid precipitate (Figure 4) are most likely associated with a P4VP-chlorine quaternary ammonium salt such as depicted in Scheme 1. To verify that the peak at ~1660 cm⁻¹ in the ATR-IR spectra of the solid precipitates (Figure 4) is associated with a zwitterionic pyridiniumepoxide adduct, we quaternized P4VP with propylene oxide. Propylene oxide is an epoxide similar in structure to epichlorohydrin except without the chlorine at the end of the epoxide chain. This chemical was chosen to test if the oxygen site of the epoxide could react and quaternize P4VP via a ring opening reaction (a ring opening polymerization reaction may also happen). Over the course of the experiment, as highlighted in the inset of Figure S14, a peak at ~1663 cm⁻¹ grows with time, which is close to the peak position of zwitterionic pyridinium-epoxide adducts reported in the literature (1655 cm⁻¹), ³⁷⁻³⁸ and close to the peak observed in the ATR-IR spectra of the solid precipitates in Figure 4 (~1663 cm⁻¹). These control experiments support our assignments of the peaks in the ATR-IR spectra of the solid precipitates to two different types of quaternized pyridinium variants: a pyridinium-chlorine quaternary ammonium salt with a characteristic infrared peak at ~1635 cm⁻¹, and a zwitterionic pyridinium-epoxide adduct with a characteristic infrared peak at ~1660 cm⁻¹.

Based on the masses of the solid precipitates (Table 1), it is unlikely that the epoxide-based adducts attached to the pyridinum ion of P4VP, 4VP, 3VP, and pyridine are monomers of epichlorohydrin. It is more likely that at least some of these adducts are oligomers of multiple epichlorohydrin repeat units with a distribution of adducts with varying chain lengths. We can estimate the average chain length of the epoxide adduct based on the mass of the solid precipitate, the mass of the catalyst (100 mg), and the total number of pyridine units in the mass of catalyst used. Accordingly, we estimate that the average chain length of the adduct, in units of

epichlorohydrin repeat units (ERU), is \sim 1.4 ERU for the solid precipitate formed in P4VP, \sim 2.4 ERU for the precipitate formed in 4VP, \sim 0.6 ERU for the precipitate formed in 3VP, and \sim 0.7 ERU for the precipitate formed in pyridine. The average chain length of the adduct on P4VP and 4VP are greater than 1, implying that a significant fraction of the adducts are oligomers of multiple epichlorohydrin repeat units.

The solid precipitate formed during quaternization of P4VP with epichlorohydrin *without* CO₂ was significantly more massive than the solid precipitate formed in the presence of 1 atm CO₂. We estimate that the average length of the epoxide adduct in the absence of CO₂ is about 4.0 ERU, compared to only ~1.4 ERU with 1 atm CO₂. This suggests that there is a competition between adduct chain growth and CO₂ uptake ultimately leading to cyclic carbonate formation, that depends on the CO₂ partial pressure. The role of this pyridinium-epoxide adduct in the cyclic carbonate synthesis reaction mechanism, and the competition between adduct chain growth and cyclic carbonate synthesis, is discussed in more detail in Section 3.4.

3.3. In-situ PM-IRAS of Chloroprene Carbonate Synthesis over P4VP and P2VP

To better understand the structure and dynamics of P4VP and P2VP under cycloaddition reaction conditions, the molecular structure of the P4VP and P2VP catalysts was characterized during exposure to epichlorohydrin/CO₂/N₂ gas mixtures using in-situ PM-IRAS. PM-IRAS is a reflectance-mode infrared spectroscopy technique with high surface sensitivity that arises from the high frequency modulation of the polarization of the incident infrared light between s- and p-polarization, and the selective absorption of s- and p-polarized light by the surface (p) and bulk gas or liquid (p + s) species. ^{45, 56} Prior to PM-IRAS measurements, the P4VP and P2VP polymer solutions were knife-cast onto reflective gold-coated slides, dried in ambient air overnight, and loaded into the reactor for PM-IRAS measurements. Epichlorohydrin/CO₂/N₂ gas mixtures were

then introduced into the reactor while the PM-IRAS spectra were recorded continuously for 4 hours of the reaction. While there are significant differences in the solvation environment of the polymers in a dried condition for in-situ PM-IRAS measurements and the liquid-phase conditions of the batch reactor studies, similar behavior is observed in both the dry condition and liquid-phase condition, as we will demonstrate below. There are also significant differences that result from the different solvation environments of the dried film and the dissolved polymer in the liquid phase. For PM-IRAS measurements, the surface of the polymer films is exposed to the gas-phase reactants. Diffusion of the reactants from the surface into the bulk of the dried film is hindered relative to the situation in the liquid phase, and most of the reaction likely occurs on the surface of the dried polymer film.

Figure S15 in the Supporting Information shows the in-situ PM-IRAS spectra of (a) P2VP and (b) P4VP collected at 0 h, 1 h, 2 h, 3 h, and 4 h of exposure to the epichlorohydrin/ CO_2/N_2 gas mixture at 57 °C. The in-situ PM-IRAS spectra display absorption bands that are associated with P2VP and P4VP, as expected, and these spectra remain mostly unchanged over the entire course of the 4 hours of exposure to the epichlorohydrin/ CO_2 gas mixture. However, there are significant changes in the PM-IRAS spectra, including the growth of new bands and the shift of P4VP/P2VP bands, which are difficult to observe in the raw PM-IRAS spectra. To more clearly show changes in the absorption bands over time, **Figure 5** shows the PM-IRAS difference spectra of (a) P2VP and (b) P4VP, which were obtained by subtracting the spectra collected prior to exposure to epichlorohydrin/ CO_2/N_2 (i.e. t=0) from the spectra collected at 1 h, 2 h, 3 h, and 4 h of epichlorohydrin/ CO_2/N_2 exposure.

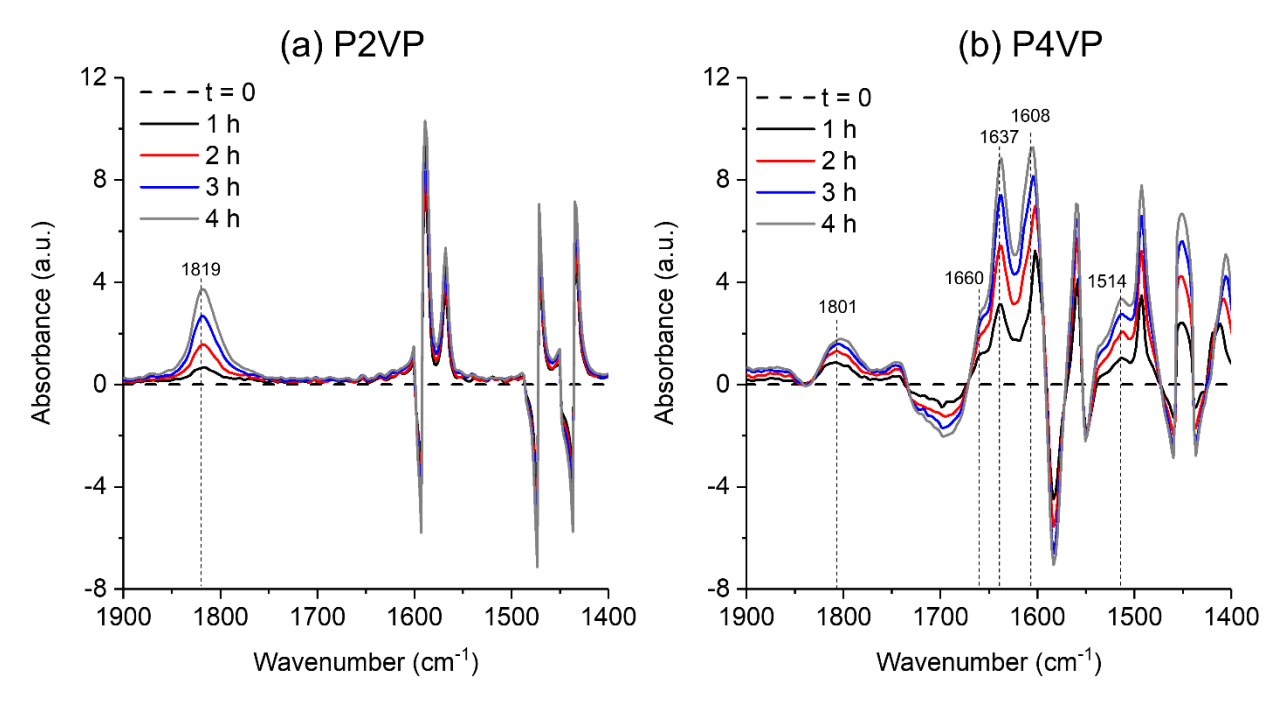


Figure 5. In-situ PM-IRAS difference spectra of (a) P2VP and (b) P4VP during exposure to epichlorohydrin/ CO_2/N_2 gas mixtures at 57 °C. The difference spectra were obtained by subtracting the spectrum collected at t = 0 h from the spectra collected at 1 h, 2 h, 3 h, and 4 h of reaction. The raw spectra are shown in Figure S14 in the Supporting Information.

The in-situ PM-IRAS difference spectra of P2VP (**Figure 5(a)**) shows a peak at 1819 cm⁻¹ that increases in intensity with increasing epichlorohydrin/CO₂/N₂ exposure time, and several derivative shaped bands in the ~1600-1200 cm⁻¹ range (see Figure S15 for full range) with positive and negative lobes. The band at 1819 cm⁻¹ is consistent with the chloroprene carbonate product, and the increase in intensity with reactant exposure time indicates that the product is accumulating on the P2VP surface. The derivative shaped bands are most likely associated with vibrational modes of the pyridine ring of P2VP; the derivative shape of the bands is due to small changes in the position of the bands, which could result from a change in the local coordination environment of the pyridine rings from interactions with epichlorohydrin, CO₂, or the cyclic carbonate product.

The difference spectra of P4VP (**Figure 5(b)**) also display many derivative-shaped bands that are likely from shifts in the positions of bands associated with P4VP from interactions with the reaction mixture. In addition to these derivative-shaped bands, there is a peak centered at ~1801 cm⁻¹, which is likely associated with the chloroprene carbonate product. There are also three relatively sharp and intense peaks centered at 1637 cm⁻¹, 1608 cm⁻¹, and 1514 cm⁻¹, which are consistent with the peak positions of the pyridinium-chlorine salt observed in the P4VP solid precipitate (Figure 4 and Scheme 1). The band associated with the pyridinium-chlorine salt at 1637 cm⁻¹ appears before the band associated with the chloroprene carbonate product at 1801 cm⁻¹ appears. This may indicate that P4VP is first quaternized by epichlorohydrin, and quaternized P4VP is the catalytically active phase for the cycloaddition reaction. There is also a clear shoulder at ~1660 cm⁻¹, which is consistent with the zwitterionic pyridinium-epoxide adduct that was also observed in the solid precipitate (Figure 4 and Scheme 1). These peaks were not observed in the in-situ PM-IRAS spectrum of P2VP, which is also consistent with our observations described in Sections 3.1 and 3.2 that the P2VP catalyst resisted quaternization and solid precipitate formation.

We do not have a reliable method for converting the PM-IRAS absorbances in Figure 5 to concentrations (of chloroprene carbonate, for example) because we cannot accurately calibrate the PM-IRAS signals to known surface concentrations. However, the changes in the intensities of the peaks over time can give some qualitative information about the evolution of the catalyst and reaction over time. The intensity of the bands associated with the chloroprene carbonate product at 1801 cm⁻¹ (for P4VP) and 1819 cm⁻¹ (for P2VP) are plotted versus reaction time in **Figure 6(a)**. Also plotted in **Figure 6(a)** is the intensity of the pyridinium-chlorine salt peak at 1637 cm⁻¹ in the in-situ PM-IRAS spectrum of P4VP during the cycloaddition reaction.

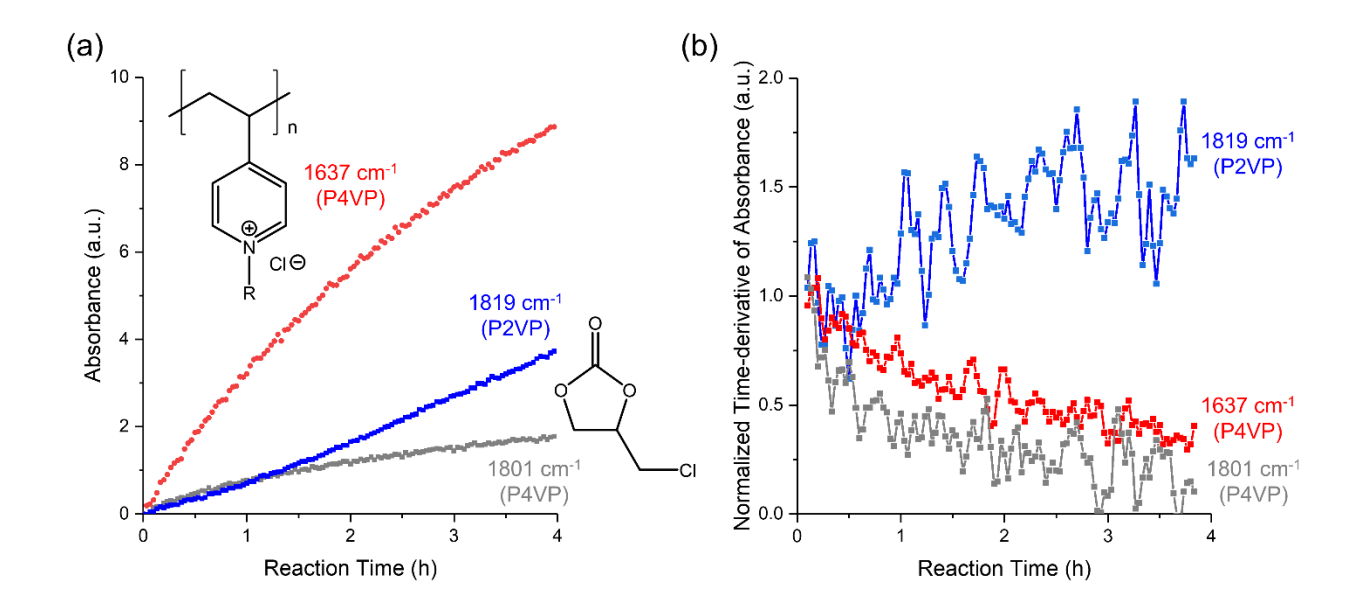


Figure 6. (a) Intensities of bands in the in-situ difference PM-IRAS spectra at 1637 cm⁻¹ (P4VP; red), 1801 cm⁻¹ (P4VP; gray), and 1819 cm⁻¹ (P2VP; blue), versus reaction time during exposure of P4VP and P2VP to epichlorohydrin/ CO_2/N_2 gas mixtures at 57 °C and 1 atm. (b) Time-derivative of the absorbance of the bands in the in-situ difference PM-IRAS spectra at 1637 cm⁻¹ (P4VP; red), 1801 cm⁻¹ (P4VP; gray), and 1819 cm⁻¹ (P2VP; blue), normalized by the time-derivate of the absorbance at t = 0 h, versus reaction time. For interpretation of the references to color in this figure caption, the reader is referred to the web version of this paper.

The chloroprene carbonate peak increases in intensity over time for both P2VP and P4VP, but with significantly different patterns. To better visualize the rate of change of these peak intensities, **Figure 6(b)** shows the time-derivative of the absorbance of the bands associated with the chloroprene carbonate product at 1801 cm⁻¹ (for P4VP) and 1819 cm⁻¹ (for P2VP), normalized by the time-derivative of absorbance at t = 0 h, versus reaction time. Although we cannot accurately quantify the rate of chloroprene carbonate production using PM-IRAS absorbance, as discussed above, this time-derivative of the absorbance can be considered roughly proportional to the instantaneous rate of chloroprene carbonate production, for the purpose of understanding trends over time. While the rate of chloroprene carbonate production decreases over time for P4VP, the rate of chloroprene carbonate production increases over time for P2VP. It is not clear why the rate

of chloroprene carbonate production over P2VP appears to increase over time, but it is possible that the build-up of the chloroprene carbonate product on the P2VP surface increases the solubility of the reactants, as hypothesized by Subramanian et al.⁴²

It is also not clear why the rate of chloroprene carbonate production over P4VP appears to decrease over time. One possible explanation is that there is a very strong interaction between the quaternized P4VP adducts and the chloroprene carbonate product, which effectively poisons the catalytically active sites. ATR-IR analysis of the solid precipitate formed in the P4VP reaction solution (Figure 3) shows that there is a significant amount of the chloroprene carbonate product incorporated into the solid precipitate, which is composed mainly of quaternized P4VP. This chloroprene carbonate product can only be removed by washing with acetone multiple times, indicating a strong intermolecular interaction between chloroprene carbonate and the quaternized P4VP. Thus, it is possible that the rate of chloroprene carbonate production over P4VP decreases over time due to poisoning of the active sites by the chloroprene carbonate product, which has a strong interaction with the quaternized P4VP active sites. This behavior was not observed with P2VP because P2VP resisted quaternization, and the chloroprene carbonate product may have a much weaker interaction with P2VP than with quaternized P4VP. The higher stretching frequency of the carbonyl stretching mode of chloroprene carbonate produced on P2VP (1819 cm⁻¹) compared to that on P4VP (1801 cm⁻¹) supports this argument that chloroprene carbonate interacts more weakly with P2VP than with P4VP.

The time-derivative of the absorbance of the band associated with the pyridinium-chlorine salt formed on the surface of P4VP at 1637 cm⁻¹, plotted in Figure 6(b), also decreases over reaction time. One possible explanation for this behavior is that the number of unquaternized P4VP sites on the surface of the film decreases over time as the sites are converted to quaternized P4VP

and poisoned by chloroprene carbonate and thus the rate of formation of the pyridinium-chlorine salt decreases over time, similar to Langmuirian adsorption behavior.

3.4. The Mechanism of Cyclic Carbonate Synthesis over P4VP, 4VP, 3VP, and pyridine

To determine whether the solid precipitates formed in the P4VP, 4VP, 3VP, pyridine, and 2VP reaction solutions are catalytically active for the cycloaddition reaction, the solid precipitate produced from the reaction between P4VP and epichlorohydrin without CO₂ was used to catalyze the cycloaddition reaction under identical conditions as that of P4VP and P2VP. The ¹H-NMR spectra before and after reaction are shown in Figure S10, and the results are summarized in Figure 2 and table 1.

Our results show that epichlorohydrin-quaternized P4VP is catalytically active for the cycloaddition reaction with an epichlorohydrin conversion of $4.9\pm0.5\%$, a chloroprene carbonate product selectivity of $54\pm4\%$, and a chloroprene carbonate production rate of 35 ± 3 mmol/mol/h. It should be mentioned that the P4VP catalyst increased in mass significantly (by a factor of ~4.5) from the quaternization by epichlorohydrin, and the mass of catalyst used (100 mg) was the same for all different catalysts presented in Figure 2 and Table 1. Therefore, the number of nitrogen sites in the quaternized P4VP catalyst was approximately $1/5^{th}$ the amount used in the other reactions listed in Table 1. Thus, the epichlorohydrin conversion over quaternized P4VP ($4.9\pm5\%$) was significantly less than that over P4VP ($11\pm3\%$), presumably because there were fewer active sites in the quaternized P4VP catalyst than in the P4VP catalyst. However, when the chloroprene carbonate production rate is normalized by the number of nitrogen active sites in the 100 mg of catalyst used, then the specific chloroprene carbonate production rate over quaternized P4VP (35 ± 3 mmol/mol/h) is much higher than that over P4VP (17 ± 4 mmol/mol/h) and all other catalysts. This estimation does not assume that the nitrogen site is the active site necessarily, but rather

assumes that there is only one active site per pyridine (pyridinium) unit, which is a reasonable assumption. Because P4VP was not present in the liquid reaction solution after the reaction, as discussed previously, this result suggests that epichlorohydrin-quaternized P4VP is the likely catalytically active species during the cycloaddition reaction over P4VP, and this quaternized P4VP catalyst has relatively high catalytic activity for the reaction, compared to the unquaternized pyridine, vinylpyridine, and polyvinylpyridine catalysts. We can reasonably assume that the precipitates formed in the 4VP, 3VP, and pyridine solutions are also catalytically active for the cycloaddition reaction, because the structure of the solid precipitates is similar according to ATR-IR spectroscopy (Figure 4).

Based on the results from this work, we propose the reaction pathways for the cycloaddition reaction over P4VP, 4VP, and pyridine displayed in **Scheme 2** (a similar mechanism is expected for 3VP, but with the nitrogen atom in the 3-position). ¹H NMR and ATR-IR analysis shows that P4VP, 4VP, 3VP, and pyridine are completely quaternized by epichlorohydrin, producing a solid precipitate composed of a zwitterionic pyridinium-epoxide adduct (step IA) and a pyridinium-chlorine quaternary ammonium salt (step IB). These zwitterionic and quaternary ammonium salt species are likely the catalytically active species in the reaction over P4VP, 4VP, 3VP, and pyridine. Thus, P4VP, 4VP, 3VP, and pyridine can be considered as catalyst pre-cursors that are converted to their quaternized counterparts that are the actual catalysts under reaction conditions.

Scheme 2. Proposed reaction pathways for chloroprene carbonate formation catalyzed by P4VP, 4VP, and pyridine via (A) a zwitterionic pyridinium-epoxide adduct or (B) a pyridinium-chlorine quaternary ammonium salt.

In path A, the negatively charged oxygen atom of the zwitterionic pyridinium-epoxide adduct attacks the less hindered carbon atom of the epoxide, forming a ring-opened complex (step IIA). CO₂ can then bind to this ring-opened complex (step IIIA) and then the target cyclic carbonate is formed by intramolecular cyclization, regenerating the zwitterionic epoxide adduct (step IVA). In path B, the chloride anion of the pyridinium-chlorine quaternary ammonium salt opens the epoxide ring through nucleophilic attack on the less sterically hindered carbon atom of the epoxide to produce an alkoxide intermediate (step IIB). The negatively charged oxygen atom of the alkoxide intermediate then binds CO₂ (step IIIB), followed by intramolecular cyclization to produce the chloroprene carbonate product and the P4VP-chlorine quaternary ammonium salt (step IVB).

As mentioned in Section 3.2, the length of the epoxide-based adduct attached to the pyridinium ion is sensitive to the CO₂ pressure and lower CO₂ partial pressures leads to larger masses of solid precipitate with longer adduct chain lengths. This can be rationalized by considering steps IIA and IIIA in the mechanism shown in Scheme 2(a). Higher CO₂ partial pressures will favor CO₂ addition to the ring opened complex (step IIIA), ultimately favoring cyclic carbonate production over adduct chain growth (step IIA). Lower CO₂ partial pressures, on the other hand, will hinder step IIIA and lead to successive addition of multiple epichlorohydrin repeat units (step IIA). The mass of the epichlorohydrin-quaternized P4VP catalyst increased during the cycloaddition reaction, from 100 mg to ~200 mg (Figure 2(a) and Table 1), which supports this proposed epoxide adduct chain growth mechanism (Scheme 2(a)).

3.5. The Mechanism of Cyclic Carbonate Synthesis over P2VP and 2VP

This work demonstrates that the amount of solid precipitate, and hence the length of the pyridinium adduct chain, is sensitive to the structure of the pyridine unit. The most striking example of this structure effect is the observation that very little solid precipitate was formed in the 2VP reaction solution and no significant amount of precipitate was formed in the P2VP reaction solution. This effect is most likely related to the degree of steric crowding at the nitrogen site of the pyridine ring. The pyridinic nitrogen sites of P2VP and 2VP are sterically crowded by the polymer backbone and the vinyl group, respectively, at the 2-position. This high degree of steric crowding at the nitrogen site could hinder the formation of epoxide-based adducts. The pyridinic nitrogen atom of P4VP, 4VP, 3VP, and pyridine, on the other hand, are much less sterically hindered than P2VP and 2VP, and consequently these catalysts form very stable adducts. The observation that 2VP formed a small, but significant, amount of precipitate whereas P2VP formed

no observable precipitate further supports this argument that steric crowding destabilizes formation of the precipitate.

This argument is further supported by our observations that the P2VP and 2VP catalysts were stable and their molecular structures were maintained over the course of the reaction. Figure 7 shows the PM-IRAS spectra of (a) pristine P2VP and (b) the P2VP reaction solution after 24 h of the cycloaddition reaction. The PM-IRAS spectrum of the P2VP reaction solution after reaction displays bands that are associated with the chloroprene carbonate product (1799 cm⁻¹, 1174 cm⁻¹, 1078 cm⁻¹) and the pristine P2VP (1585 cm⁻¹, 1566 cm⁻¹, 1471 cm⁻¹, 1433 cm⁻¹, 1147 cm⁻¹, 1048 cm⁻¹, 991 cm⁻¹). While there is a small band centered at ~1626 cm⁻¹ in the PM-IRAS spectrum of the post-reaction P2VP solution, which is likely associated with a pyridinium-chlorine quaternary ammonium salt, similar to the one observed with P4VP, 4VP, and pyridine at ~1635 cm⁻¹, only a small amount of the P2VP is quaternized and the bands associated with pyridine vibrations of P2VP are mostly retained. This is consistent with ¹H-NMR results (Figures S5 and S7) that also show P2VP and 2VP remain in the liquid reaction mixture whereas P4VP, 4VP, and pyridine were not detected in the liquid after the reaction (Figure S4, S6, and S9). Thus, while P4VP, 4VP, 3VP, and pyridine were completely converted to a pyridinium-chlorine quaternary ammonium salt and/or zwitterionic pyridinium-epoxide adducts during the cycloaddition reaction, P2VP and 2VP resist quaternization, most likely due to the high degree of steric crowding of the nitrogen atom at the 2-position of P2VP and 2VP.

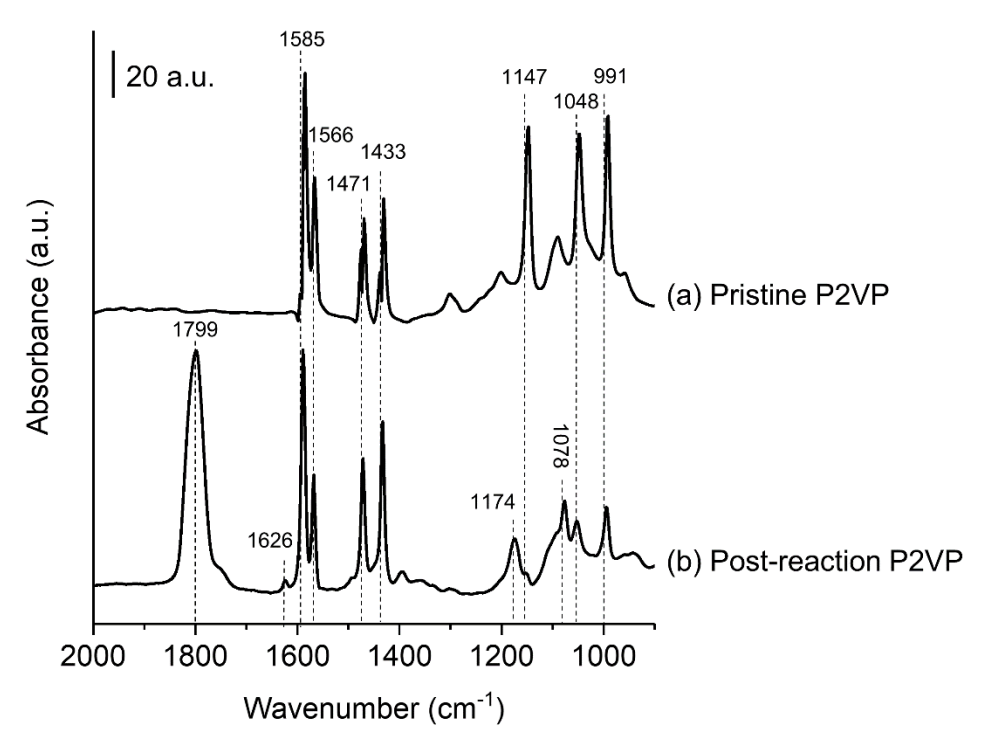
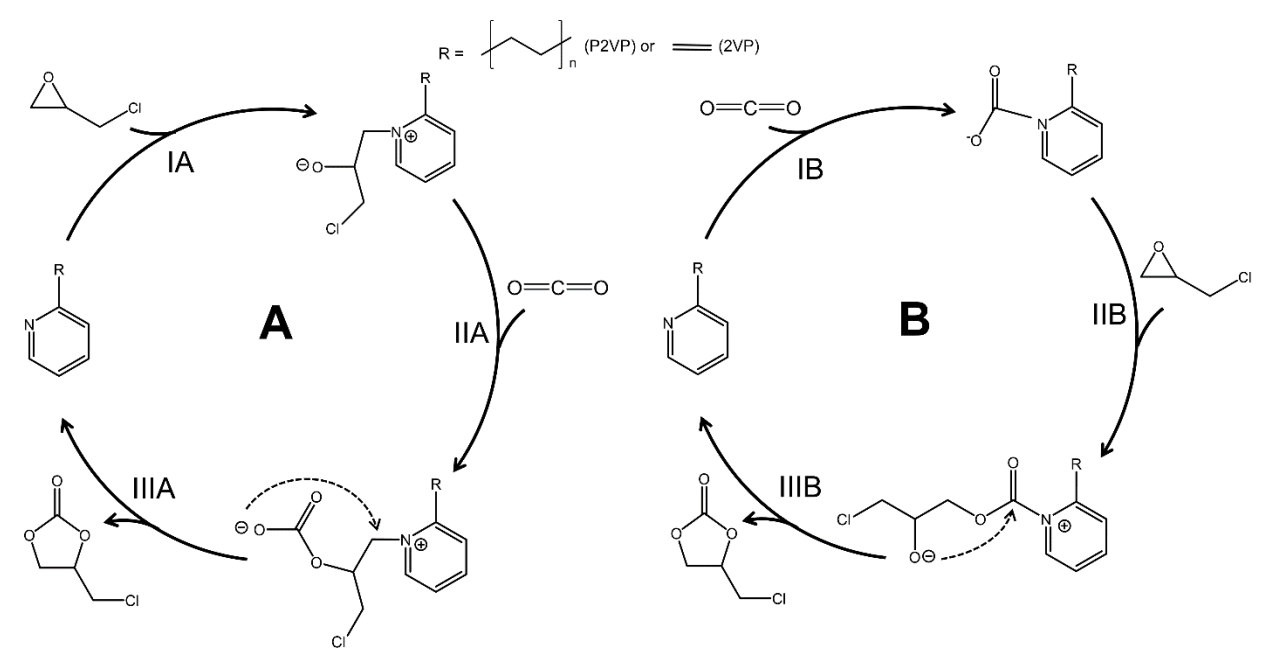


Figure 7. PM-IRAS spectra of (a) pristine P2VP and (b) the P2VP reaction solution after 24 of the cycloaddition reaction at 57 °C with 1 atm CO₂.

Thus, we propose the reaction pathways for P2VP and 2VP shown in **Scheme 3**, which are similar to pathways commonly proposed for single-component nucleophilic catalysts.³⁴ In pathway A, the lone pair of electrons of the nitrogen atom of P2VP or 2VP attack the less hindered carbon atom of epichlorohydrin, forming a zwitterionic pyridinium-epoxide adduct (step IA). The negatively charged oxygen atom of this zwitterionic adduct then binds CO₂ (step IIA) and intramolecular cyclization (step IIIA) produces the chloroprene carbonate product and regenerates the P2VP active site. This pathway is similar to the pathway proposed for P4VP, 4VP, 3VP, and pyridine in Scheme 2(a). However, the high degree of steric hindrance at the pyridinic nitrogen atom of P2VP and 2VP hinders chain growth of the adduct (step IIA in Scheme 2(a)), and favors CO₂ addition to ultimately lead to cyclic carbonate production and regeneration of the P2VP or 2VP catalyst.



Scheme 3. Proposed reaction pathways for chloroprene carbonate formation catalyzed by P2VP and 2VP in which the first step is either (A) epoxide activation or (B) CO₂ activation.

Another possible pathway to chloroprene carbonate synthesis over P2VP and 2VP is pathway B in scheme 3 in which the first step is the interaction of the CO₂ with the lone pair of electrons of the nitrogen atom of P2VP to form a carbamate anion (step IB). The negatively charged carbamate ion then attacks the less hindered carbon atom of the epoxide to open the epoxide ring (step IIB). Finally, intramolecular cyclization produces the chloroprene carbonate product and regenerates the P2VP catalyst. Lim et al.⁵⁷ postulated, based on density functional theory calculations, that the pyridine carbamate anion (PyCOO⁻), similar to the carbamate anion formed in step IB of the proposed pathway B, is an important intermediate in the mechanism of CO₂ reduction by pyridine. The pyridine carbamate anion has also been observed experimentally⁵⁸⁻⁵⁹ albeit under extreme conditions (e.g., by high-energy electron impact of pyridine/CO₂ mixtures in supersonic expansion⁵⁹ or by the reaction of pyridine vapor with CO₂ in an ionized, supersonic entrainment ion source⁵⁸). Thus, under the experimental conditions investigated in this work (57 °C,

1 atm CO₂), it is unlikely that the carbamate anion is an intermediate in the cycloaddition reaction, and pathway A or some other pathway is more likely. Future work will focus on identifying the intermediates in the cycloaddition reaction over pyridine, vinylpyridines, and poly(vinylpyridines).

4. Conclusions

This work demonstrates that steric crowding at the ring nitrogen atom of pyridine-based catalysts significantly influences the rate, selectivity, and mechanism of cyclic carbonate synthesis from the cycloaddition of CO₂ with an epoxide. Catalysts with unhindered access to the ring nitrogen (P4VP, 4VP, 3VP, pyridine) are completely quaternized by the epichlorohydrin reactant during the cycloaddition reaction, transforming the pyridine-based catalysts into zwitterionic pyridinium-epoxide adducts and pyridinium-chlorine quaternary ammonium salts that precipitate out of solution. The solid precipitates composed of zwitterionic pyridinium adducts and pyridinium-chlorine salts are catalytically active for the cycloaddition reaction and are likely the catalytically active phase during the cycloaddition reaction over P4VP, 4VP, 3VP, and pyridine. Catalysts with hindered access to the ring nitrogen (P2VP, 2VP), on the other hand, resist quaternization due to the high degree of steric hindrance at the ring nitrogen atom that hinders quaternization. These sterically crowded catalysts are much more stable than unhindered analogs. This work also demonstrates that the structure of organic N-nucleophilic base catalysts is dynamic under reaction conditions, which highlights the importance of in-situ/operando characterization. These insights have significant implications for the rational design of green catalysts with high activity, selectivity, and stability for the CO₂ cycloaddition reaction.

Supporting Information

Photograph of batch reactor flask and mass change of rubber stopper; photographs of reaction solutions; liquid ¹H-NMR spectra of reactions solutions; comparison of pK_a and carbonate production rate; procedure for synthesis of pure chloroprene carbonate; synthesis of HCl-quaternized P4VP; quaternization of P4VP by propylene oxide; in-situ PM-IRAS raw spectra.

Acknowledgments

This work was funded through NSF CAREER (CBET-2144362). We would also like to thank the Material Characterization Facility and the Center for Environmental Science and Technology at Notre Dame.

References

- 1. North, M.; Pasquale, R.; Young, C., Synthesis of cyclic carbonates from epoxides and CO₂. *Green Chem.* **2010**, *12* (9), 1514-1539.
- 2. Cokoja, M.; Wilhelm, M. E.; Anthofer, M. H.; Herrmann, W. A.; Kühn, F. E., Synthesis of Cyclic Carbonates from Epoxides and Carbon Dioxide by Using Organocatalysts. *ChemSusChem* **2015**, *8* (15), 2436-2454.
- 3. Sathish, M.; Sreeram, K. J.; Raghava Rao, J.; Unni Nair, B., Cyclic Carbonate: A Recyclable Medium for Zero Discharge Tanning. ACS Sus. Chem. Eng. 2016, 4 (3), 1032-1040.
- 4. Lawrenson, S. B.; Arav, R.; North, M., The greening of peptide synthesis. *Green Chem.* **2017**, *19* (7), 1685-1691.
- 5. North, M.; Villuendas, P., A Chiral Solvent Effect in Asymmetric Organocatalysis. *Org. Lett.* **2010**, *12* (10), 2378-2381.
- 6. Yan, C.; Yao, Y.-X.; Chen, X.; Cheng, X.-B.; Zhang, X.-Q.; Huang, J.-Q.; Zhang, Q., Lithium Nitrate Solvation Chemistry in Carbonate Electrolyte Sustains High-Voltage Lithium Metal Batteries. *Ang. Chem. Int. Ed.* **2018**, *57* (43), 14055-14059.
- 7. Gómez, J. E.; Cristòfol, À.; Kleij, A. W., Copper-Catalyzed Enantioselective Construction of Tertiary Propargylic Sulfones. *Ang. Chem. Int. Ed.* **2019**, *58* (12), 3903-3907.
- 8. Guo, K.; Kleij, A. W., Cu-Catalyzed Synthesis of Tetrasubstituted 2,3-Allenols through Decarboxylative Silylation of Alkyne-Substituted Cyclic Carbonates. *Org. Lett.* **2020**, *22* (10), 3942-3945.
- 9. Guo, W.; Gómez, J. E.; Cristòfol, À.; Xie, J.; Kleij, A. W., Catalytic Transformations of Functionalized Cyclic Organic Carbonates. *Ang. Chem. Int. Ed.* **2018**, *57* (42), 13735-13747.
- 10. Grignard, B.; Gennen, S.; Jérôme, C.; Kleij, A. W.; Detrembleur, C., Advances in the use of CO₂ as a renewable feedstock for the synthesis of polymers. *Chem. Soc. Rev.* **2019**, *48* (16), 4466-4514.
- 11. Yadav, N.; Seidi, F.; Crespy, D.; D'Elia, V., Polymers Based on Cyclic Carbonates as Trait d'Union Between Polymer Chemistry and Sustainable CO₂ Utilization. *ChemSusChem* **2019**, *12* (4), 724-754.
- 12. Bobbink, F. D.; van Muyden, A. P.; Dyson, P. J., En route to CO₂-containing renewable materials: catalytic synthesis of polycarbonates and non-isocyanate polyhydroxyurethanes derived from cyclic carbonates. *Chem. Commun.* **2019**, *55* (10), 1360-1373.
- 13. Monie, F.; Grignard, B.; Thomassin, J.-M.; Mereau, R.; Tassaing, T.; Jerome, C.; Detrembleur, C., Chemo- and Regioselective Additions of Nucleophiles to Cyclic Carbonates for the Preparation of Self-Blowing Non-Isocyanate Polyurethane Foams. *Ang. Chem. Int. Ed.* **2020**, *59* (39), 17033-17041.
- 14. Guo, L.; Lamb, K. J.; North, M., Recent developments in organocatalysed transformations of epoxides and carbon dioxide into cyclic carbonates. *Green Chem.* **2021**, *23* (1), 77-118.
- 15. Alves, M.; Grignard, B.; Mereau, R.; Jerome, C.; Tassaing, T.; Detrembleur, C., Organocatalyzed coupling of carbon dioxide with epoxides for the synthesis of cyclic carbonates: catalyst design and mechanistic studies. *Catal. Sci. Technol.* **2017**, *7* (13), 2651-2684.
- 16. Kulal, N.; Vasista, V.; Shanbhag, G. V., Identification and tuning of active sites in selected mixed metal oxide catalysts for cyclic carbonate synthesis from epoxides and CO₂. *J. CO₂ Util.* **2019**, *33*, 434-444.

- 17. Marciniak, A. A.; Lamb, K. J.; Ozorio, L. P.; Mota, C. J. A.; North, M., Heterogeneous catalysts for cyclic carbonate synthesis from carbon dioxide and epoxides. *Curr. Opinion Green Sus. Chem.* **2020**, *26*, 100365.
- 18. Caló, V.; Nacci, A.; Monopoli, A.; Fanizzi, A., Cyclic Carbonate Formation from Carbon Dioxide and Oxiranes in Tetrabutylammonium Halides as Solvents and Catalysts. *Org. Lett.* **2002**, *4* (15), 2561-2563.
- 19. Wang, J.-Q.; Dong, K.; Cheng, W.-G.; Sun, J.; Zhang, S.-J., Insights into quaternary ammonium salts-catalyzed fixation carbon dioxide with epoxides. *Catal. Sci. Technol.* **2012**, *2* (7), 1480-1484.
- 20. Bobbink, F. D.; Dyson, P. J., Synthesis of carbonates and related compounds incorporating CO₂ using ionic liquid-type catalysts: State-of-the-art and beyond. *J. Catal.* **2016**, *343*, 52-61.
- 21. Xu, B.-H.; Wang, J.-Q.; Sun, J.; Huang, Y.; Zhang, J.-P.; Zhang, X.-P.; Zhang, S.-J., Fixation of CO₂ into cyclic carbonates catalyzed by ionic liquids: a multi-scale approach. *Green Chem.* **2015**, *17* (1), 108-122.
- 22. Girard, A.-L.; Simon, N.; Zanatta, M.; Marmitt, S.; Gonçalves, P.; Dupont, J., Insights on recyclable catalytic system composed of task-specific ionic liquids for the chemical fixation of carbon dioxide. *Green Chem.* **2014**, *16* (5), 2815-2825.
- 23. He, Q.; O'Brien, J. W.; Kitselman, K. A.; Tompkins, L. E.; Curtis, G. C. T.; Kerton, F. M., Synthesis of cyclic carbonates from CO₂ and epoxides using ionic liquids and related catalysts including choline chloride–metal halide mixtures. *Catal. Sci. Technol.* **2014**, *4* (6), 1513-1528.
- 24. Moya, C.; Sabater, V.; Yagüe, G.; Larriba, M.; Palomar, J., CO₂ conversion to cyclic carbonates catalyzed by ionic liquids with aprotic heterocyclic anions: DFT calculations and operando FTIR analysis. *J. CO₂ Util.* **2018**, *28*, 66-72.
- 25. Comerford, J. W.; Ingram, I. D. V.; North, M.; Wu, X., Sustainable metal-based catalysts for the synthesis of cyclic carbonates containing five-membered rings. *Green Chem.* **2015**, *17* (4), 1966-1987.
- 26. Paddock, R. L.; Nguyen, S. T., Chemical CO₂ Fixation: Cr(III) Salen Complexes as Highly Efficient Catalysts for the Coupling of CO₂ and Epoxides. *J. Amer. Chem. Soc.* **2001**, *123* (46), 11498-11499.
- 27. Fuchs, M. A.; Zevaco, T. A.; Ember, E.; Walter, O.; Held, I.; Dinjus, E.; Döring, M., Synthesis of cyclic carbonates from epoxides and carbon dioxide catalyzed by an easy-to-handle ionic iron(iii) complex. *Dalton Transact.* **2013**, *42* (15), 5322-5329.
- 28. Buyukcakir, O.; Je, S. H.; Talapaneni, S. N.; Kim, D.; Coskun, A., Charged Covalent Triazine Frameworks for CO₂ Capture and Conversion. *ACS Appl. Mater. Interf.* **2017**, *9* (8), 7209-7216.
- 29. Sun, Q.; Aguila, B.; Perman, J.; Nguyen, N.; Ma, S., Flexibility Matters: Cooperative Active Sites in Covalent Organic Framework and Threaded Ionic Polymer. *J. Amer. Chem. Soc.* **2016**, *138* (48), 15790-15796.
- 30. Dai, Z.; Sun, Q.; Liu, X.; Bian, C.; Wu, Q.; Pan, S.; Wang, L.; Meng, X.; Deng, F.; Xiao, F.-S., Metalated porous porphyrin polymers as efficient heterogeneous catalysts for cycloaddition of epoxides with CO₂ under ambient conditions. *J. Catal.* **2016**, *338*, 202-209.
- 31. Liu, F.; Huang, K.; Wu, Q.; Dai, S., Solvent-Free Self-Assembly to the Synthesis of Nitrogen-Doped Ordered Mesoporous Polymers for Highly Selective Capture and Conversion of CO₂. *Adv. Mater.* **2017**, *29* (27), 1700445.
- 32. Talapaneni, S. N.; Buyukcakir, O.; Je, S. H.; Srinivasan, S.; Seo, Y.; Polychronopoulou, K.; Coskun, A., Nanoporous Polymers Incorporating Sterically Confined N-Heterocyclic

- Carbenes for Simultaneous CO₂ Capture and Conversion at Ambient Pressure. *Chem. Mater.* **2015**, 27 (19), 6818-6826.
- 33. Cho, W.; Shin, M. S.; Hwang, S.; Kim, H.; Kim, M.; Kim, J. G.; Kim, Y., Tertiary amines: A new class of highly efficient organocatalysts for CO₂ fixations. *J. Indust. Eng. Chem.* **2016**, *44*, 210-215.
- 34. Natongchai, W.; Luque-Urrutia, J. A.; Phungpanya, C.; Solà, M.; D'Elia, V.; Poater, A.; Zipse, H., Cycloaddition of CO₂ to epoxides by highly nucleophilic 4-aminopyridines: establishing a relationship between carbon basicity and catalytic performance by experimental and DFT investigations. *Org. Che. Front.* **2021**, *8* (3), 613-627.
- 35. Roshan, K. R.; Palissery, R. A.; Kathalikkattil, A. C.; Babu, R.; Mathai, G.; Lee, H.-S.; Park, D.-W., A computational study of the mechanistic insights into base catalysed synthesis of cyclic carbonates from CO₂: bicarbonate anion as an active species. *Catal. Sci. Technol.* **2016**, *6* (11), 3997-4004.
- 36. Suleman, S.; Younus, H. A.; Khattak, Z. A. K.; Ullah, H.; Elkadi, M.; Verpoort, F., Cocatalyst and solvent free nitrogen rich triazole based organocatalysts for cycloaddition of CO₂ into epoxide. *Molec. Catal.* **2020**, *493*, 111071.
- 37. D'Elia, V.; Ghani, A. A.; Monassier, A.; Sofack-Kreutzer, J.; Pelletier, J. D. A.; Drees, M.; Vummaleti, S. V. C.; Poater, A.; Cavallo, L.; Cokoja, M.; Basset, J.-M., et al. Dynamics of the NbCl₅-Catalyzed Cycloaddition of Propylene Oxide and CO₂: Assessing the Dual Role of the Nucleophilic Co-Catalysts. *Chem. Eur. J.* **2014**, *20* (37), 11870-11882.
- 38. Dutta, B.; Sofack-Kreutzer, J.; Ghani, A. A.; D'Elia, V.; Pelletier, J. D. A.; Cokoja, M.; Kühn, F. E.; Basset, J.-M., Nucleophile-directed selectivity towards linear carbonates in the niobium pentaethoxide-catalysed cycloaddition of CO₂ and propylene oxide. *Catal. Sci. Technol.* **2014**, *4* (6), 1534-1538.
- 39. Monassier, A.; D'Elia, V.; Cokoja, M.; Dong, H.; Pelletier, J. D. A.; Basset, J.-M.; Kühn, F. E., Synthesis of Cyclic Carbonates from Epoxides and CO₂ under Mild Conditions Using a Simple, Highly Efficient Niobium-Based Catalyst. *ChemCatChem* **2013**, *5* (6), 1321-1324.
- 40. Beyzavi, M. H.; Stephenson, C. J.; Liu, Y.; Karagiaridi, O.; Hupp, J. T.; Farha, O. K., Metal–Organic Framework-Based Catalysts: Chemical Fixation of CO₂ with Epoxides Leading to Cyclic Organic Carbonates. *Front. Energy Research* **2015**, *2*, 1-10.
- 41. Lu, B.-B.; Yang, J.; Liu, Y.-Y.; Ma, J.-F., A Polyoxovanadate–Resorcin[4]arene-Based Porous Metal–Organic Framework as an Efficient Multifunctional Catalyst for the Cycloaddition of CO₂ with Epoxides and the Selective Oxidation of Sulfides. *Inorg. Chem.* **2017**, *56* (19), 11710-11720.
- 42. Subramanian, S.; Park, J.; Byun, J.; Jung, Y.; Yavuz, C. T., Highly Efficient Catalytic Cyclic Carbonate Formation by Pyridyl Salicylimines. *ACS Appl. Mater. Interf.* **2018**, *10* (11), 9478-9484.
- 43. Rehman, A.; Saleem, F.; Javed, F.; Ikhlaq, A.; Ahmad, S. W.; Harvey, A., Recent advances in the synthesis of cyclic carbonates via CO₂ cycloaddition to epoxides. *J. Envir. Chem. Eng.* **2021**, *9* (2), 105113.
- 44. Rycke, N. D.; Berionni, G.; Couty, F.; Mayr, H.; Goumont, R.; David, O. R. P., Synthesis and Reactivity of Highly Nucleophilic Pyridines. *Org. Lett.* **2011**, *13* (3), 530-533.
- 45. Lee, G.; Easa, J.; Jin, R.; Booth, A.; O'Brien, C. P., Enhancing the surface sensitivity of insitu/operando characterization of palladium membranes through polarization modulation and synthesis of optically smooth palladium thin films. *J. Membr. Sci.* **2021**, *637*, 119605.

- 46. Shimizu, S.; Watanabe, N.; Kataoka, T.; Shoji, T.; Abe, N.; Morishita, S.; Ichimura, H., Pyridine and Pyridine Derivatives, *Ullmann's Encyclopedia of Industrial Chemistry*. Wiley-VCH Verlag GmbH & Co. KGaA, Weinheim, Germany, 2000, DOI: 10.1002/14356007.a22 399.
- 47. Tantavichet, N.; Pritzker, M. D.; Burns, C. M., Proton uptake by poly(2-vinylpyridine) coatings. *J. Appl. Polym. Sci.* **2001**, *81* (6), 1493-1497.
- 48. Chanda, M.; O'Driscoll, K. F.; Rempel, G. L., Cyanide detoxification by selective ion exchange with protonated poly(4-vinyl pyridine). *J. Chem. Tech. Biotech. Chem. Tech.* **1983**, *33* (2), 97-108.
- 49. Matsuo, A.; Hasegawa, S.; Takano, S.; Tsukuda, T., Electron-Rich Gold Clusters Stabilized by Poly(vinylpyridines) as Robust and Active Oxidation Catalysts. *Langmuir* **2020**, *36* (27), 7844-7849.
- 50. Human Metabolome Database (Accessed December 5, 2022). https://hmdb.ca/metabolites/HMDB0061887.
- 51. Mavronasou, K.; Zamboulis, A.; Klonos, P.; Kyritsis, A.; Bikiaris, D. N.; Papadakis, R.; Deligkiozi, I., Poly(vinyl pyridine) and Its Quaternized Derivatives: Understanding Their Solvation and Solid State Properties. *Polymers* **2022**, *14* (4), 804.
- 52. Groppo, E.; Uddin, M. J.; Zavorotynska, O.; Damin, A.; Vitillo, J. G.; Spoto, G.; Zecchina, A., Exploring the Chemistry of Electron-Accepting Molecules in the Cavities of the Basic Microporous P4VP Polymer by in situ FTIR Spectroscopy. *J. Phys. Chem. C* **2008**, *112* (49), 19493-19500.
- 53. Topuzogullari, M., Microwave assisted quaternization of poly(4-vinylpyridine) with 1-bromohexane. *J. Polym. Res.* **2018**, *25* (8), 188.
- 54. Dong, P.; Cui, K.; Xu, F.; Jiang, T.; Ma, Z., Synthesis of new ionic crosslinked polymer hydrogel combining polystyrene and poly(4-vinyl pyridine) and its self-healing through a reshuffling reaction of the trithiocarbonate moiety under irradiation of ultraviolet light. *Polymer Int.* **2018**, *67* (7), 868-873.
- 55. Khalig, N. G., Investigation of the catalytic activity of poly(4-vinylpyridine) supported iodine as a new, efficient and recoverable catalyst for regioselective ring opening of epoxides. *RSC Adv.* **2012**, *2* (8), 3321-3327.
- 56. Lee, G.; Go, D. B.; O'Brien, C. P., Direct Observation of Plasma-Stimulated Activation of Surface Species Using Multimodal In Situ/Operando Spectroscopy Combining Polarization-Modulation Infrared Reflection-Absorption Spectroscopy, Optical Emission Spectroscopy, and Mass Spectrometry. *ACS Appl. Mater. Interf.* **2021**, *13* (47), 56242-56253.
- 57. Lim, C.-H.; Holder, A. M.; Musgrave, C. B., Mechanism of Homogeneous Reduction of CO₂ by Pyridine: Proton Relay in Aqueous Solvent and Aromatic Stabilization. *J. Amer. Chem. Soc.* **2013**, *135* (1), 142-154.
- 58. Kamrath, M. Z.; Relph, R. A.; Johnson, M. A., Vibrational Predissociation Spectrum of the Carbamate Radical Anion, C₅H₅N-CO₂⁻, Generated by Reaction of Pyridine with (CO₂)m⁻. *J. Amer. Chem. Soc.* **2010**, *132* (44), 15508-15511.
- 59. Han, S. Y.; Chu, I.; Kim, J. H.; Song, J. K.; Kim, S. K., Photoelectron spectroscopy and ab initio study of mixed cluster anions of $[(CO_2)_{1-3}(Pyridine)_{1-6}]^-$: Formation of a covalently bonded anion core of $(C_5H_5N-CO_2)^-$. *J. Chem. Phys.* **2000**, *113* (2), 596-601.

TOC Graphic